1993

Thermal Analysis of Spirally Wound Li/BCX and Li/$SOCl_2$ Cells

E. E. Kalu
Texas A & M University - College Station

Ralph E. White
University of South Carolina - Columbia, white@cec.sc.edu

Publication Info

Journal of the Electrochemical Society, 1993, pages 23-31.

Publisher's link: http://dx.doi.org/10.1149/1.2056095
DOI: 10.1149/1.2056095

Thermal Analysis of Spirally Wound Li/BCX and Li/$SOCl_2$ Cells

E. E. Kalu*,[a] and R. E. White*

Department of Chemical Engineering, Texas A&M University, College Station, Texas 77843-3122

ABSTRACT

A thermal analysis of Li/BCX and high rate Li/$SOCl_2$ cells is presented. The thermal model developed was used to study the effect of ambient temperature of discharge (0-40°C) on Li/BCX cells discharged at the same rate. The model predictions show that ambient temperature of discharge was critical in thermal management of the cell. For forced convection cooled cells, the model predicted that ambient temperature near room temperature (25°C) was required to achieve the lowest maximum temperature rise in the cell. Inclusion of the effects of reaction products to the model predictions showed that a constant composition assumption may be misleading. Heat transfer through the spiral constituted a smaller fraction of the total heat dissipation from the cell. In a comparison of the thermal performance of high rate Li/$SOCl_2$ cell with Li/BCX cell, the model predicted a higher temperature rise in the Li/$SOCl_2$ cell (assuming the temperature rise behaves linearly with discharge current) if both cells were discharged at the same rate.

The nature of heat exchange with the ambient when a battery is discharged is utmost in the minds of most battery engineers and designers.[1-5] Ever since the Li/$SOCl_2$ cell was described in 1973,[6] attempts have been made to design a Li/$SOCl_2$ cell that is safe and maintains all the attractive features associated with the lithium/thionyl couple.

Two complementary ways have been used to address the thermal problems associated with lithium/thionyl chloride based cells. One approach views the cell problem from a thermal/thermodynamic point, the problem of the cell is ascribed to a thermal runaway that arises from resistance to heat conduction.[3,4] The other approach ascribes the thermal problem of the cell to the intermediate products of the electrochemical processes, a kinetic approach.[7-9] Consequently, efforts have been made through thermal modeling to examine the influence of cell design variables on the heat removal from the cell.[3,4,10,11] Such an effort leads to recommendations for more efficient thionyl chloride based cell designs. The kinetic view may have led to the development of a thionyl chloride based battery system in 1979, the Li/BCX cell.[7] The Li/BCX cell contains bromine chloride which is believed to modify the intermediate products of the reaction process. The performance of the Li/BCX cell may be better than that of the Li/$SOCl_2$ cell. However, in spite of its relatively good characteristics little information is known about the thermal properties of the Li/BCX cell. Recently the thermoneutral potential of the Li/BCX cell was measured experimentally and compared to that of the Li/$SOCl_2$ cell.[12,13]

Modeling provides faster information on a system than the traditional experimental approach. However, for a model to be useful, the important physical/chemical processes occurring in the system must be accounted for. Thermal models of the Li/$SOCl_2$ cell previously presented have been used to describe the system using different simplifying assumptions.[3,4,10,11] However, in these previous thermal models, the description has not accounted for the effects of the reaction products and porous cathode characteristics adequately. The influence of LiCl deposit on the cathode performance has been verified experimentally.[14] Using experimentally determined thermal parameters, this work aims to understand the performance of Li/BCX and Li/$SOCl_2$ cells. Though a model similar to the present work has been presented for the Li/$SOCl_2$ cell,[4] this work differs from the work on Li/$SOCl_2$ in Ref. 4 in that the effects of reaction products are considered (approximate system assumptions made) and furthermore, a comparison between the thermal behavior of the Li/BCX cell and the high rate Li/$SOCl_2$ cell is made.

The objective of this work was to carry out a thermal analysis of DD Li/BCX primary cell using experimentally determined thermal parameters. It also compared the thermal behavior of the Li/BCX and Li/$SOCl_2$ cells. The model predictions are used to compare the thermal behavior of Li/BCX cells discharged at the same rate but at different ambient temperatures.

Previous Models

Thermal modeling has been applied to the study of battery systems.[10,15,16] Bernardi *et al.*[15] used thermodynamic and kinetic arguments to present a general energy balance for a battery. The treatment was rigorous and involved a knowledge of concentration changes of the active species. The model assumed *a priori*, a flat temperature profile for the battery interior, which changes with time. Ogata *et al.*[17] carried out a mathematical analysis of the heat balance in a vertical water electrolysis cell. The development of the governing equation was based on the principle of entropy production (a consequence of heat, mass, charge transfer, and chemical reaction.)[18] Lee *et al.*[16] used a three-dimensional thermal model to analyze the thermal behavior of rechargeable nickel/iron batteries for electric vehicle application. The preceding models treated the cell interior as a homogeneous medium with effective average properties.

The models presented that specifically addressed the thermal behavior of Li/$SOCl_2$ based cells include the models of Parnell and Szpak,[3] Szpak *et al.*,[10] Cho,[5] Cho and Halpert,[19] and Evans and White.[4] The model of Parnell and Szpak[3] was used to consider a thin-disk-shaped Li/$SOCl_2$ cell and to consider the elementary processes that take place during cell discharge. Processes that involve changes in porosity or other material properties were included in the model. The model results show the need to account for temperature and concentration dependence of the thermophysical properties. They indicate that for a cathode limited cell, the prime heat source resides in the cathode structure when the cathode porosity becomes less than 20%. A similar model to Parnell and Szpak's[3] was presented by Szpak *et al.*[10] to account for catastrophic thermal runaway. The model was used to consider the thermal runaway as due to a cell defect rather than to an explosion. A numerical solution to simultaneous energy and material balance equations was used to predict the time and position dependence of temperature and concentration profiles. The model agreement with experiment was excellent, thereby suggesting that thermal runaway is a consequence of a cell component defect.

Cho and Halpert[19] presented a model for a spirally wound Li/$SOCl_2$ cell in which a homogeneous approximation was used. The resulting governing equation for this model can be solved analytically to obtain the temperature of the cell as a function of time. In a further effort on the Li/$SOCl_2$ thermal model, Cho and Halpert[11] and Cho[5] used electrical circuit equivalent principles in modeling the thermal resistance of the cell components. The major con-

* Electrochemical Society Active Member.
[a] Present address: Monsanto, St. Louis, MO 63167.

clusion of these investigations was that 91% of the total heat transfer occurs radially. They also demonstrated that based on the first generation of the high rate D-cell, C/1.5 discharge rate could be carried out under normal conditions.

Evans and White[4] used both the Parnell and Szpak[3] and Szpak *et al.*[10] approaches in their model of a $Li/SOCl_2$ cell. Results obtained for circular and core approximations were compared to those of a spiral model. The thermal model did not include the effects of the new products formed as a result of the electrochemical processes. Such products as LiCl and S affect the porosity of the cathode material, while dissolved sulfur dioxide and sulfur in the electrolyte change the thermophysical properties of the electrolyte.

Experiments also have demonstrated the importance of the porosity of carbon material in cell performance.[14,20] Klinedinst concluded that the porosity of the carbon black material has an important bearing on the $Li/SOCl_2$ cell capacity.[14] The cathode utilization efficiency increases linearly with increasing porosity. This is expected, since apparently the LiCl produced deposits within the porous carbon. Other workers have found that the cell capacity is related to pore volume of the cathode.[21] Because small pores are easily blocked, the use of pore formers in the cathode manufacturing processes results in an improved cell performance.[14] A comprehensive thermal model of $Li/SOCl_2$ based batteries must take into account the changes that occur in the cell due to the consumption of lithium and the swelling of the electrode matrix. Szpak and Driscoll have shown that expansion of the cathode matrix must be incorporated in any design of the cell.[20]

A Li/BCX thermal model has not been presented. Although the Li/BCX cell has the same active components as the $Li/SOCl_2$ cell, (except for the presence of BrCl in the Li/BCX cell), the Li/BCX cell behaves in a safer manner than the $Li/SOCl_2$ cell.[22] The differences in their thermal behavior must be due to the presence of BrCl. Thus a comparative study of thermal models of the Li/BCX and $Li/SOCl_2$ cells can be useful for the design of an improved thionyl chloride based cell system.

The model presented here is similar to the one presented by Evans and White for a $Li/SOCl_2$ cell.[4] However, unlike the model in Ref. 4, the present model for the Li/BCX cell accounted for the dependence of the cathode porosity on LiCl and sulfur deposits in a simple manner. Furthermore, the effects of the products of the reaction on the thermophysical properties of the electrolyte were investigated. The model compares the thermal behavior of a Li/BCX cell discharged at different ambient temperatures.

Model Development

The overall reactions that take place in a Li/BCX cell and a $Li/SOCl_2$ cell are given respectively by Eq. 1 and 2

$$24Li + 8SOCl_2 + 8BrCl \rightarrow 24LiCl + 2SO_2Br_2 + 2SO_2 + 2S + S_2Br_2 + Br_2 \quad [1]$$

$$4Li + 2SOCl_2 \rightarrow 4LiCl + S + SO_2 \quad [2]$$

The main insoluble product of these reactions is LiCl; however, depending on temperature and level of saturation, sulfur eventually precipitates. The precipitated solids block the pores of the cathode. Furthermore, the thermal properties of the precipitates are different from either those of the parent cathode material or the electrolyte that fills the void. The other components of the product of reaction are mostly soluble in the solvent/electrolyte system except for sulfur dioxide which has a low solubility in the solvent. A thermal model in which the effects of these products of reaction are included may be helpful in elucidating the performance differences between $Li/SOCl_2$ and Li/BCX cells. To include the effects of these materials, a combined material and energy balance of the system must be carried out. Alternatively, a worst case information on the role of these materials can be obtained by the adoption of a simple approach in which the energy balance is solved completely but with assumed stoichiometric equivalents of the species. This approach does not give an exact solution to the problem, but it does provide a better approximation to the solution relative to that obtained without consideration of the concentration effects. This approach was used in the present model.

Cho and Halpert[19] and Evans and White[4] solved the energy balance equation *i.e.*, equivalent to a constant composition assumption. Assuming conduction as the only means of heat transfer in the cell, the temperature distribution in the k_{th} region of the cell is given by

$$\rho_k c_{p,k} \frac{\partial T}{\partial t} = \nabla \cdot (f_k \nabla T) + \sum_j q_{vj} \quad [3]$$

While ρ_k stands for the density and $c_{p,k}$ the heat capacity of region k, f_k stands for its thermal conductivity. The heat generation per unit volume (q_{vj}) can be replaced by using either the experimentally measured heat rate or by using a knowledge of the different heat sources in the cell. The heat sources may include energy changes arising from intrinsic sources such as the heat produced by thermally activated exothermic reactions. The other sources of heat in a discharging cell are made up of heat generated by polarization and entropy effects. The heat due to polarization (q_p) and entropy effects (q_s) per unit volume, is given by the product of current flow and the difference between the thermoneutral potential and load voltage as in Eq. 4

$$q_v = \frac{q_p + q_s}{V_{cell}} = \frac{I(E_{etp} - E_l)}{V_{cell}} \quad [4]$$

where V_{cell} is the volume of the cell. In this work, the effective thermoneutral potential (E_{etp}) for the cell was determined without separating the noncurrent producing heat sources from the current producing heat sources. Thus the use of Eq. 4 in 3 assumes a negligible noncurrent producing heat source.

The time-dependent change in cathode porosity as LiCl and S are deposited is given by[23,24]

$$\frac{\partial \varepsilon}{\partial t} = \sum_i \sum_k \frac{S_{i,k} V_{bi} a}{n_k F} i_k \quad [5]$$

where v_{bi} is the partial molar volume of species i, and $s_{i,k}$ is the stoichiometric coefficient of species i in electrochemical reaction k when written in the form

$$\sum_i s_{i,k} M_i^{zi} \rightarrow n_k e^- \quad [6]$$

The specific surface area, a, is given by

$$a = a^\circ \left(1 - \left(\frac{\varepsilon_o - \varepsilon}{\varepsilon_o}\right)^\chi\right) \quad [7]$$

where a° is the initial specific active surface area, ε_o is the initial porosity, and χ is a parameter determined experimentally. This value adjusts the surface area of electrode available for electrochemical reactions, which varies with deposit buildup. Thus, the parameter measures the salt loading or choking of the active electrode. The value of this parameter depends on the physical nature of the deposits, the larger deposits have a needle-like appearance. If for simplicity, a value of $\chi = 1$ is adopted, an exponential relationship between porosity and time is obtained. The thermal properties of the solvent/electrolyte system change with time due to the dissolved products of the reaction. The resulting thermal property (L_m) can be approximated by

$$L_m = \Sigma X_i L_{m,i} \quad [8]$$

where X_i is the mole fraction or quantity-fraction of i in the solvent/electrolyte/reaction product mixture. Finally, the boundary conditions and initial conditions for these equations are presented. For the temperature, a convection boundary condition was used

$$-f_k \frac{\partial T}{\partial x} n_x - f_k \frac{\partial T}{\partial y} n_y = h_u (T_w - T_{sur}) \quad [9]$$

where T_w and T_{sur} are the temperature of the outer wall of cell and the ambient temperature, respectively. T_w is a function of x, y, and t; and h_u is the heat transfer coefficient which was assumed constant for the present problem. The initial temperature (T_0) was taken to be equal to T_w since each cell was equilibrated long enough (up to 10 h) to acquire the temperature of the surroundings.

Solution Procedure

The procedure used by Evans and White for construction and approximation of the spirals in their TOPAZ2D model of the Li/$SOCl_2$ cell in Ref. 4 was adopted in this work.

However, the problem was solved using a finite element package from IMSL called PDE/PROTRAN.[25] The PDE/PROTRAN uses triangular elements. A program was written for generating the nodes of the triangles. An approximation for the DD-Li/BCX cell spiral model region is shown in Fig. 1. The dimensions are in meters. The spiral model region was better approximated with a large number of triangular elements. For the DD-Li/BCX cell, 3 1/2 wounds approximated the design while the high rate D-Li/$SOCl_2$ cell was approximated with 8 1/2 wounds. The specifications for the Li/BCX and Li/$SOCl_2$ cells are given in Table I. In the model of Evans and White,[4] the cell specifications were not consistent with the discharge information used. For instance, the Li/$SOCl_2$ cell was approximated with 3 1/2 wounds and was said to have been discharged at 4.0 A. The high rate Li/$SOCl_2$ cell developed by JPL has 8 1/2 wounds[11,19] and can be discharged at the high rate of 4.0 A. It is rather the DD-Li/BCX cell which is designed with 3 1/2 wounds and not the high rate D-Li/$SOCl_2$ cell modeled in Ref. 4.

As pointed out by Szpak and Venkatasetty,[26] an appropriate model of the thionyl chloride based cell must account for the temperature and concentration dependence of the thermophysical properties of the cell parameters. Unfortunately, such data are lacking for the thionyl chloride based cells. In Table II, the thermophysical properties of the different cell components are presented, including the dependence (if known) of these parameters on temperature. The cells in this work were discharged under a forced convection cooling, during which a constant temperature was maintained outside the cell. Similarly, in Table III, the thermophysical parameters of the reaction products are presented. The model parameters are the heat transfer coefficient and the effective thermoneutral potential. Since the dependence of the thermoneutral potential of the cells on temperature is not too strong, a constant thermoneutral potential for each cell type was assumed between 0° to 60°C. The effective thermoneutral potentials for the Li/BCX cell and the Li/$SOCl_2$ cell were, respectively, 4.0 V and 3.84 V. Since an exact value of the heat transfer coefficient was not known, a value of heat transfer coefficient greater than that often assumed for natural convection,[4,10] was used for most of the cases reported here.

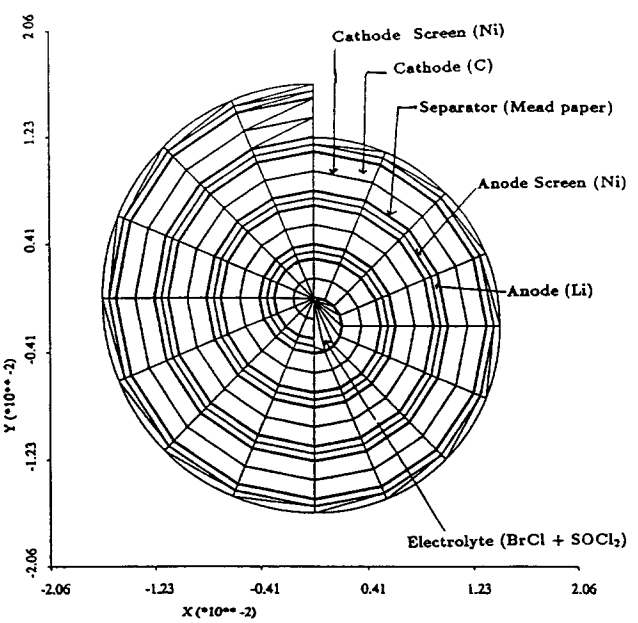

Fig. 1. The spiral model region of Li/BCX cell using PDE/PROTRAN.

Table I. Cell specifications for a typical DD-Li/BCX and high rate D-Li/$SOCl_2$ cells.

Cell specification	Value Li/BCX	Value Li/$SOCl_2$	Ref.
Anode thickness	0.4572 mm	0.127 mm	29
Cathode thickness	1.397 mm	0.635 mm	29
Separator thickness	0.127 mm	0.127 mm	29
Screen thickness	0.0762 mm	0.0762 mm	29
Cell case thickness	0.7874 mm	0.7874 mm	29
Porosity of cathode	0.85	0.85	29
Porosity of separator	0.80	0.80	29
Number of wraps	3 1/2	8 1/2	5, 30
Volume	9.787×10^4 mm^3	4.906×10^4 mm^3	29

Table II. Thermophysical properties of the cell materials used in the model.

Material	Density (kg/m^3)	Thermal conductivity (W/m, K)	Specific heat (J/kg, K)	Ref.
Anode	519.074	71.1	3492.0	29
Cathode	1950.0	23.8	712.0	4, 3, 10
Separator	0.4238	0.242	963.0	29
Screen (Ni)	8900.0	90.5	444.0	29
Electrolyte (BCX)	1730	0.175[a]	925/1600ζ	29
Electrolyte (Li/$SOCl_2$)	1660	0.143	921/1590[a]	29, 3, 4

[a] Estimated, ζ values at 20/100°C, respectively.

Table III. Thermophysical properties of the reaction products.

Material	Density (kg/m^3)	Thermal conductivity (W/m, K)	Specific heat (J/kg, K)	Ref.
LiCl	2068.0	0.005	1183/1210ζ	31, 32
S	2046.0	0.2927	739.7/785.6ζ	31, 32
SO_2	5.54	0.00816	1069.9[a]	31, 33
SO_2Br_2	2667.0	0.22	1038.0	31, 33, 32
S_2Br_2	2635.0	0.215	532.18	31
Br_2	3119.0	0.0049	473.33	32

ζ values at 20/100°C, respectively.
[a] $c_p = 502.7 + 0.346T + 0.0054T^2$.

Initially, Eq. 3 was solved with a constant concentration or composition assumption. Thus, the effects of LiCl and sulfur precipitates (in the pores of the porous cathode) and reaction products (mixed with the electrolytes) on the temperature profile were not considered. To assess the importance of the reaction products on model predictions, an assumption was made regarding reactant/product distribution. At the cutoff voltage point, a certain fraction of the active electrolyte/solvent was assumed to have been consumed. Except when otherwise stated, 75% extent of reaction at the cutoff voltage was assumed for model predictions in this work. With this assumption, we obtained an approximate concentration/time or mole fraction/time relation for the electrolyte/solvent system. A linear or an exponential form of relation can be assumed. For the present results, the mole fraction of the active material was assumed to decrease exponentially.

Since the thermal parameters of the components of the starting reactants were not known individually, a single value for the whole mixture was used. Furthermore, it was assumed that the stoichiometric molar fractions of each reacting component were used. For instance, in the Li/BCX cell system, 8 moles of $SOCl_2$ and 8 moles of BrCl react to produce 2 moles of SO_2, etc., if the reaction goes to comple-

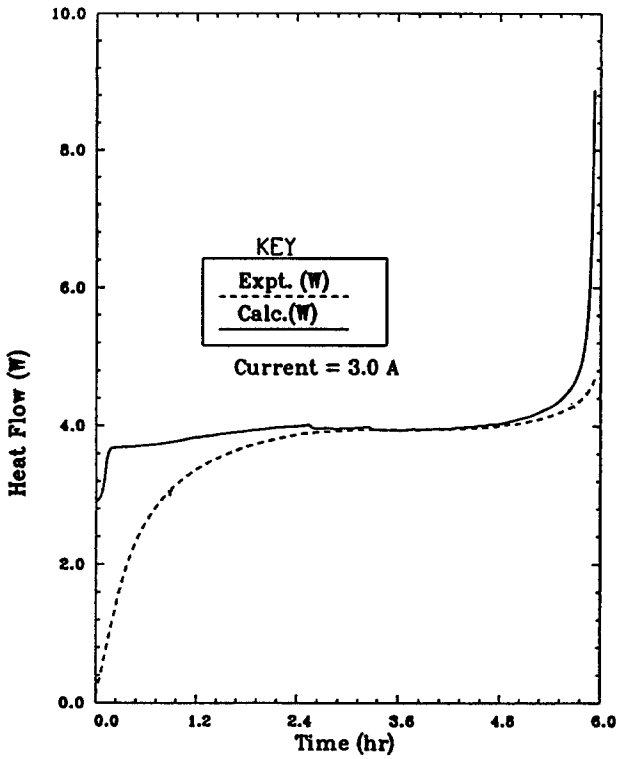

Fig. 2. Comparison of measured heat rate against heat flow computed with an average thermoneutral potential (Li/BCX cell).

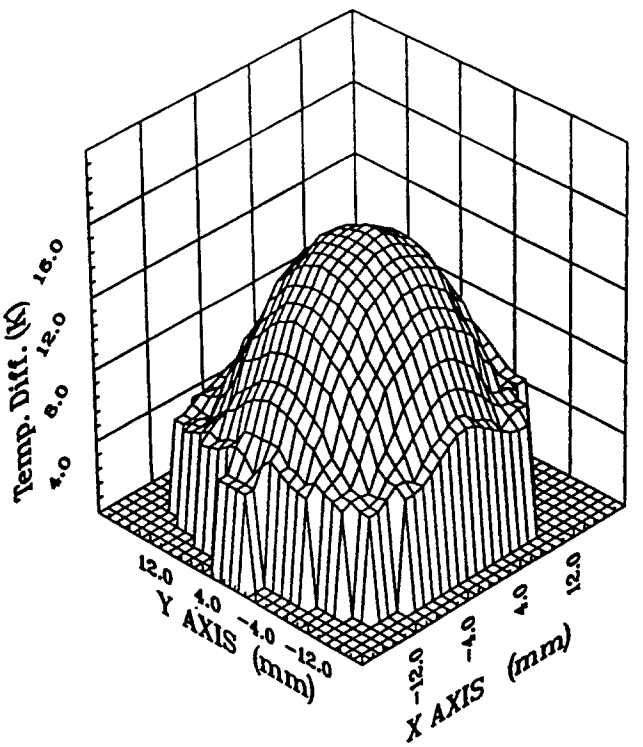

Fig. 3. Predicted temperature rise profile for a DD-BCX cell at 80 min into the discharge (2.0 A discharge rate) and an ambient temperature of 20°C.

tion. The starting material was assumed to contain an equivalent of 8 moles $SOCl_2$ and 8 moles BrCl. The method used in the measurement of the heat rate is described in Ref. 12. Fixing the extent of reaction at the cutoff voltage subsequently fixes the mole fraction of each species at the initial and final time of operation. Equation 8 was used to calculate the thermal property of interest for the reaction product mixture at any time. This approach was not meant to be exact and accurate, but was employed to emphasize the errors inherent in the extreme case of constant composition assumption for the duration of the reaction. Note that for the $Li/SOCl_2$ cell, the initial starting mixture assumed in the model development contained only the solvent, $SOCl_2$.

Results and Discussion

Figure 2 shows a comparison of the measured heat rate against that predicted using a modified form of Eq. 4 for the Li/BCX cell. The close agreement between the calculated heat rate and the experimentally determined value justifies both the use of this equation and an average value for the thermoneutral potential in the model.

A typical result of the model application in which the porosity was assumed constant (*i.e.*, the effects of LiCl, S and other by-products were not taken into account) is shown in Fig. 3. The result shows that the distribution of the temperature rise was uniform. Furthermore, the average temperature increased from 20°C to approximately 31°C at the maximum point (discharge time = 80 min). The result was obtained for a moderate forced convection cooling.

From the literature,[14,27] it is well documented that the porosity of the carbon cathode plays an important role in cell performance. The decrease in cathode porosity arises as a consequence of precipitation of insoluble materials such as LiCl and S (after exceeding its saturation point in the solvent/electrolyte system) in the pores of the cathode. An accurate species material balance is required to incorporate the porosity effects realistically in this model. Such a material balance not only includes the effects of the porosity changes, but also accounts for the effects of the reaction products on the model. The role of these products is important in thermal predictions or else a prediction of any substantial thermal differences between $Li/SOCl_2$ and Li/BCX cells may not be realized. Such a difference, however, exists in practice. Although Li/BCX has a higher effective thermoneutral potential (4.0 V) than the $Li/SOCl_2$ cell (3.84 V) (experimentally obtained in this work), experience has shown that the Li/BCX cell has a better safety record than the $Li/SOCl_2$ cell.[7] This contradicts what is expected of these cells based on their thermoneutral potential. It is the belief of the authors, therefore, that the intermediate and final products of the chemical/electrochemical reaction processes do have an impact on the thermal behavior of the cell system. The inclusion and consideration of the reaction products are justified.

Since an accurate material balance is outside the scope of this work, an approximate approach as already outlined was used to investigate the effect of the worst-case concentration effects on the predicted temperature distribution within the cell. Figure 4 shows a comparison of temperature rise profiles predicted by the model in the spatial direction Y, when the products of reaction were incorporated in the model. The results in Fig. 4 show that the inclusion of the products of the reaction leads to a significant thermal resistance within the cell interior and near the boundary region as indicated by sharp temperature drops. When these products were not considered, lower temperature rise and an almost uniform thermal resistance within the cell were predicted. The breaks observed in the figures correspond to the wraps (with different thermal properties) in the spirally wound cell. T_0 in the figures corresponds to the ambient temperature.

In Fig. 5, the effects of ambient temperature of discharge on the predicted maximum temperature rise are presented. Initially, the maximum temperature rise predicted decreased as the ambient temperature increased (*i.e.*, temperature rise at $40 < 20 < 0$°C). But after about 30 min into the discharge, the maximum temperature rise predicted for the ambient temperature at 40°C was in between the values at 0 and 20°C. As shown in the figure, the maximum temperature rise at 20°C ambient increased sluggishly relative to the other two temperatures. The reason for the predicted behavior is not clear. However, the figure suggests that an optimum ambient temperature of discharge for the Li/BCX

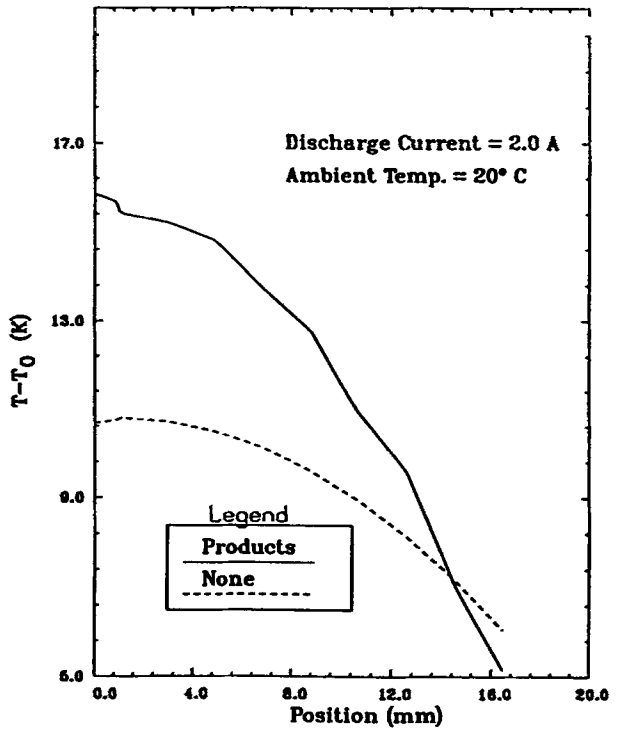

Fig. 4. Predicted radial temperature rise profile in a DD-Li/BCX cell for two model assumptions (discharge time = 80 min).

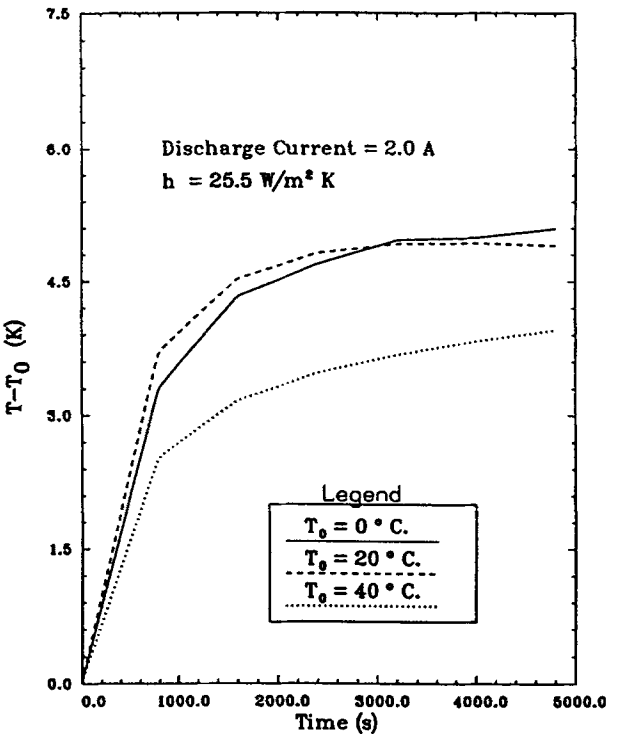

Fig. 6. Predicted ambient temperature (T_o) and time effects on the minimum temperature rise inside the spiral of a Li/BCX cell.

cell can be defined. According to the figure, such an optimum ambient temperature results in the lowest maximum temperature rise in the interior of the cell. From the comparison, such an optimum ambient temperature should be near room temperature (25°C).

The effects of the ambient temperature on the minimum temperature rise is shown in Fig. 6. Initially, a rapid increase in the minimum temperature was predicted for all three ambient temperatures considered. The model predicted highest minimum temperature rise at an ambient of 20°C and the lowest at 40°C ambient. Whereas the minimum temperature rise at 20 and 0°C ambient continues to increase very slightly after 15 min into the discharge, the minimum temperature rise at 40°C increased at a slower rate. At 60 min into the discharge, the minimum temperature rise for the 0°C ambient increased beyond the values at the other two temperatures. In contrast to the earlier observation regarding optimum ambient temperature of discharge, Fig. 6 suggests discharging the cell at temperatures higher than 40°C to obtain the lowest minimum temperature rise. However, the temperature of importance in regard to safety is the maximum temperature rise. Thus discharging the cell near or at room temperature (25°C) seems appropriate. The minimum temperature occurred at the cell wall.

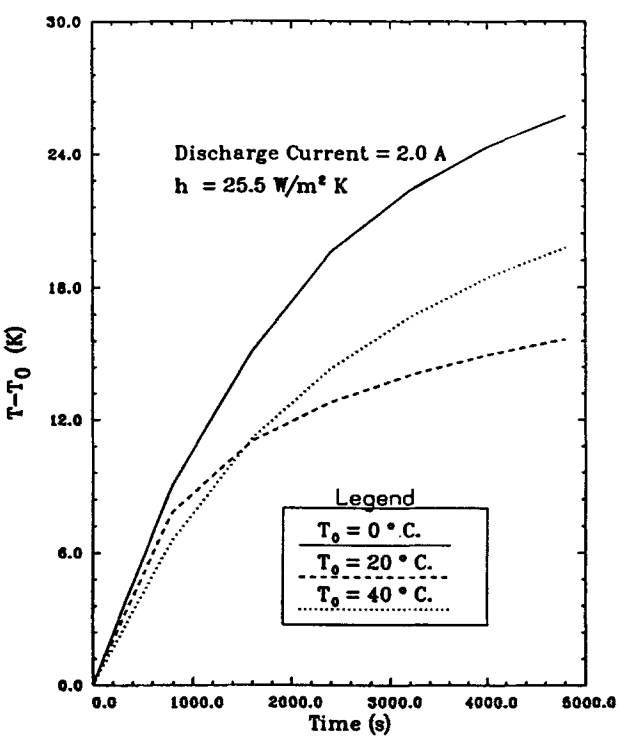

Fig. 5. Effect of ambient temperature (T_o) and time on the predicted maximum temperature rise for a Li/BCX cell.

Figure 7 compares the spatial temperature profiles in the Y-direction as predicted by the model. The predictions show that the maximum temperature rise near the center of the cell was as high as 26°C at an ambient temperature of 0°C. The high thermal resistance at the center of the cell is attributed to the low thermal conductivity of the electrolyte which occupies the center of the cell. The relative temperature drop from the cell interior to the exterior was 22 (0 ambient), 16 (40 ambient), and 12°C (20°C ambient). The predicted results compare reasonably well with results obtained experimentally for C-cells ($Li/SOCl_2$) by Abraham *et al.*[28] The sharp drops seen in the temperature profiles are attributed to changes in the thermal properties of the material (as one moves out radially), and also because heat is transported along the spirals. The inclusion of precipitates and reaction products in the model affects the predicted heat flux. Although a substantial amount of heat flux was predicted to be transported radially, the model also predicted heat flux along the spirals. This heat flux is probably due to an increased (thermal) resistance to energy transport across the carbon cathode as the pores are blocked by solid reaction precipitates. When the precipitates and other reaction products are not accounted for, the model predicted only radial heat flux as shown in Fig. 8.

The overall shape of the curves remained the same with different cooling rates. The model is capable of predicting the effects of cooling rate on temperature rise within the cell (Fig. 9). The temperature rise in the cell decreases as the cooling rate increases.

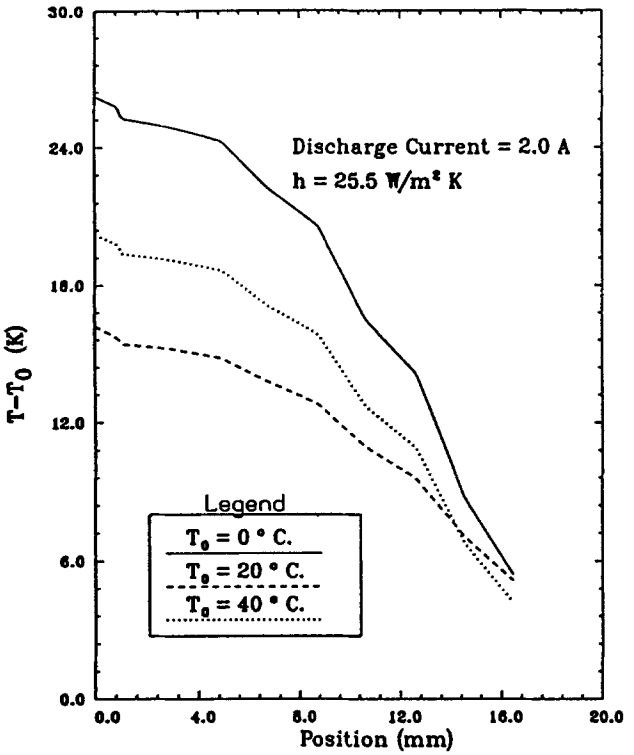

Fig. 7. Predicted radial temperature rise distributions in a Li/BCX cell at different ambient conditions (T_0) at 80 min into the discharge.

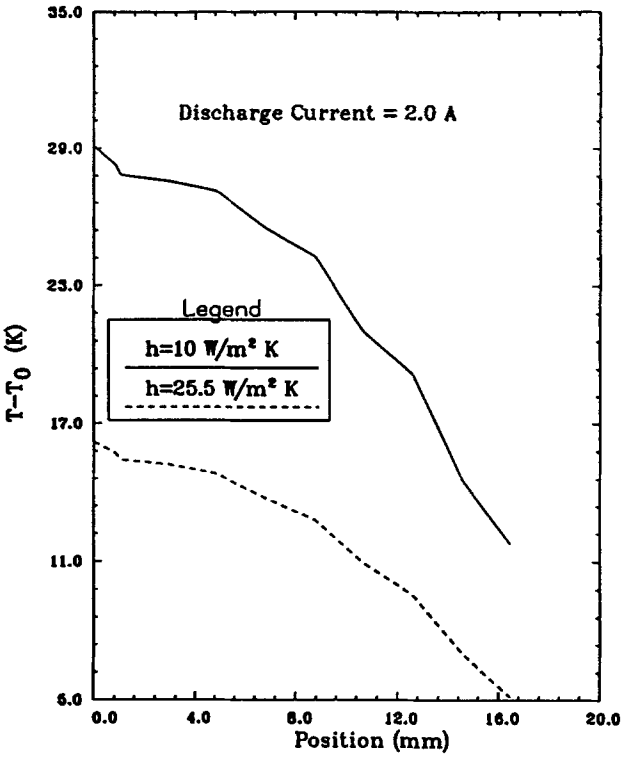

Fig. 9. Effect of cooling rate on predicted radial temperature distributions for a Li/BCX cell (80 min into discharge), ambient temperature 20°C.

Next, we consider the effect that the inclusion of solid precipitates and reaction products has on the predicted temperature rise. The predictions for the quantity of minimum and maximum temperature rise at 0°C ambient are shown in Fig. 10. The model predicted lower maximum temperature rise and a higher minimum temperature rise when precipitates and products were neglected. The thermal properties of the reaction products (including the reactants) have a profound effect on temperature rise during cell discharge. To improve the thermal behavior of the Li/BCX cell system, either a change in the thermal properties of the reaction products is effected or an appropriate cooling or potting system to remove much of the generated heat is designed. Changing the thermal properties of reaction products can mean only the introduction of exotic additives in the cell system.

Although the Li/BCX and Li/$SOCl_2$ cells were discharged at different rates, a comparison of their predicted internal temperature increase can be useful in elucidating the differences in the thermal characteristics of the two cell systems. Such a comparison at an ambient temperature of 20°C is shown in Fig. 11. The model predicted both a higher

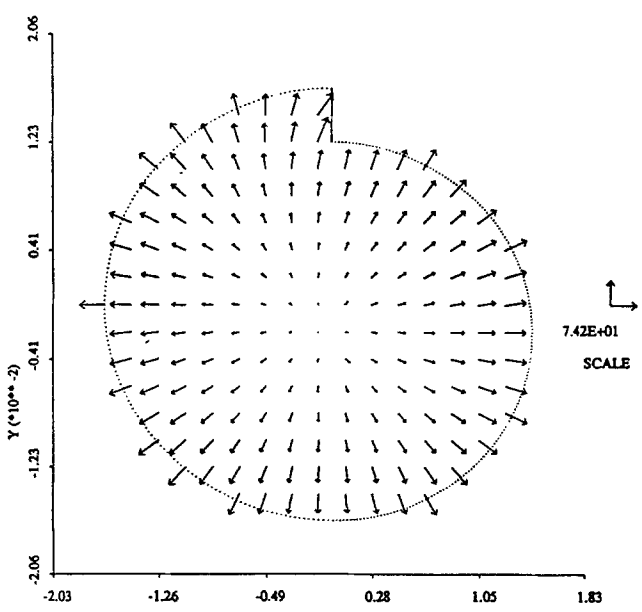

Fig. 8. Predicted heat flux for a Li/BCX cell at 0°C ambient temperature without the effects of precipitates and products.

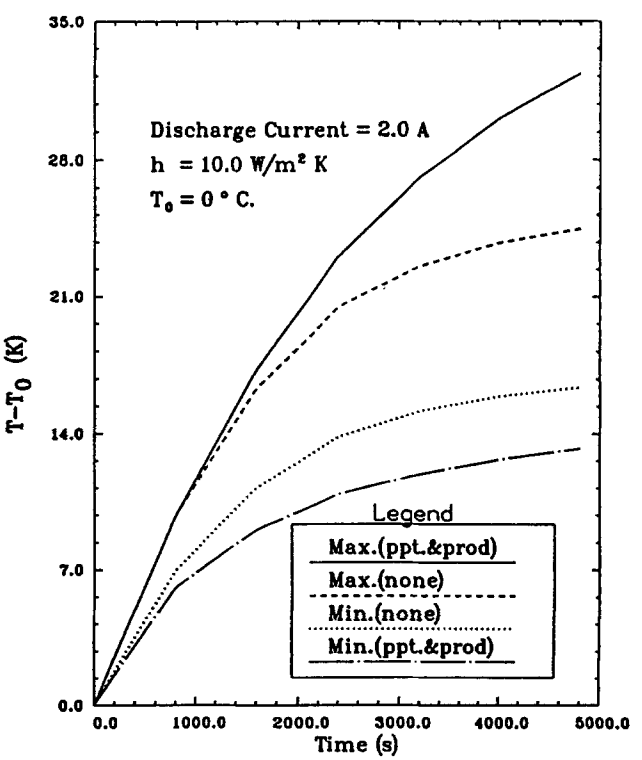

Fig. 10. Effect of reaction products and precipitates on the model predictions for Li/BCX cell.

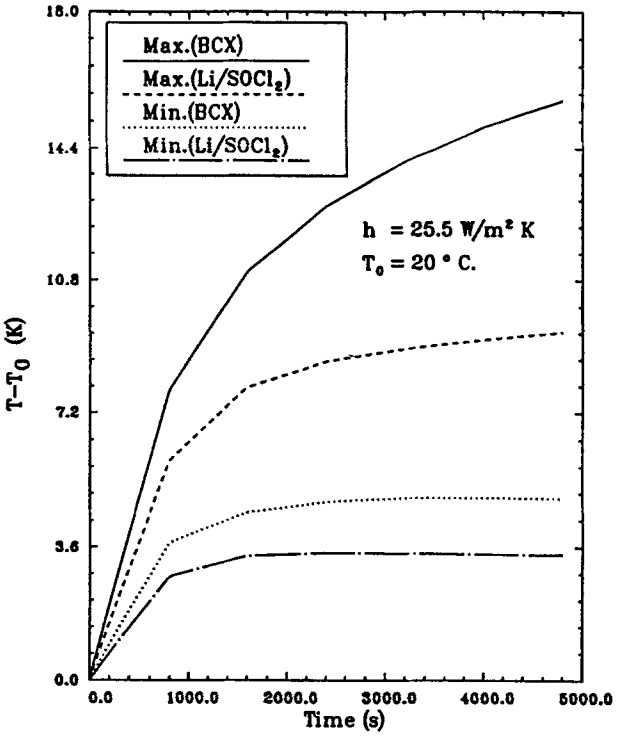

Fig. 11. Predicted variations in the maximum and minimum temperature of a Li/BCX cell (5.37 mA/cm²) and Li/$SOCl_2$ (1.89 mA/cm²) with the depth of discharge.

maximum and a higher minimum temperature increase for the Li/BCX cell. This is expected since the Li/BCX cell was discharged at a higher rate. Assuming that the discharge rate is proportional (in a linear manner) to the predicted temperature increase and based on the results in Fig. 11, the maximum temperature increase predicted for the Li/BCX cell suggests that at 1.0 A rate, the Li/BCX cell maximum internal temperature increase is lower than that predicted for the Li/$SOCl_2$ cell (at 1.0 A). The model also predicts a higher temperature increase for the Li/$SOCl_2$ cell at 2.0 A rate relative to that predicted for the Li/BCX cell in Fig. 11. The implication of this analysis is that, under the same discharge conditions, the maximum interior temperature increase for the Li/$SOCl_2$ cell can be higher compared to the temperature increase in the Li/BCX cell. The most probable cause of such a difference may be the reaction products. A higher temperature increase in the Li/$SOCl_2$ cell relative to the Li/BCX cell is in agreement since the Li/BCX cell has a better safety record than the Li/$SOCl_2$ cell.

The bulk heat capacities of the Li/BCX and Li/$SOCl_2$ cells were measured experimentally. Accurate heat capacity and thermal conductivity are needed to predict the temperature distributions within the cell. However, the determination of the thermal conductivities of the cells was not carried out since that was beyond the scope of the present work. To use the experimentally determined heat capacity data, the cell was assumed to behave as a homogeneous medium whose thermophysical properties are the average of the properties of all the cell components. The weights of the more important components were known and the core region properties were calculated using Eq. 8. The thermal conductivity was the only thermophysical property obtained by the use of Eq. 8. The average mass fractions for the major components of the Li/BCX and Li/$SOCl_2$ cells are shown in Table IV.

The reaction products were included in the model by assuming an equimolar mixture of $SOCl_2$ and BrCl as the starting electrolyte/solvent solution in the case of the Li/BCX cell. The starting electrolyte/solvent solution was taken to contain only the solvent (*i.e.*, the electrolyte salt, $LiAlCl_4$, was not accounted for) for cases of evaluating the initial moles of solvent used. We also assumed that the reaction follows the stoichiometric equation, and that the extent of reaction at the cutoff voltage was known. A typical result obtained for the Li/BCX cell at 20°C is compared to the full spiral model predictions (Fig. 12). A similar result for the Li/$SOCl_2$ cell is presented in Fig. 13. Both figures show that the core approximation predicts a uniform temperature, which means that there is a negligible temperature difference between the maximum (interior) and minimum (exterior) temperatures. Whereas in Fig. 12 (Li/BCX cell), the core approximation predicts a larger temperature increase than is the case in the spiral assumption, the opposite is true in Fig. 13 (Li/$SOCl_2$ cell). This is not clear except to speculate that the differences in the chemistry of the reactions may have contributed to the results. For both cells the minimum temperature increase that was predicted by the spiral approximation was below that obtained by the core model. The overall shape of the temperature-time curves shows a qualitative agreement with experimental temperature-time curves[28] where an initial rise in temperature (during the early polarization process) is followed by a plateau where generated heat is equal to heat removed (a steady-state condition), and finally, a sharp increase in temperature as the active material in the cell is consumed. For the results presented here, the temperature is followed till the beginning of the plateau. The information obtained from this result was sufficient for verification of the model capabilities and the cell thermal characteristics of interest.

Finally, the effects of the assumed extent of the reaction on model predictions for two cases are compared in Fig. 14.

Table IV. Mass fractions of the important cell specifications for typical DD-Li/BCX and high rate D-Li/$SOCl_2$ cells.

Cell specification	Mass fraction Li/BCX	Mass fraction Li/$SOCl_2$	Ref.
Anode	0.04375	0.0287	29
Cathode	0.04525	0.0470	29
Separator	1.4×10^{-5}	2.75×10^{-5}	29
Screen	4.359×10^{-3}	9.28×10^{-3}	29
Electrolyte	0.44288	0.3908	29
Cell case	0.462	0.508	29

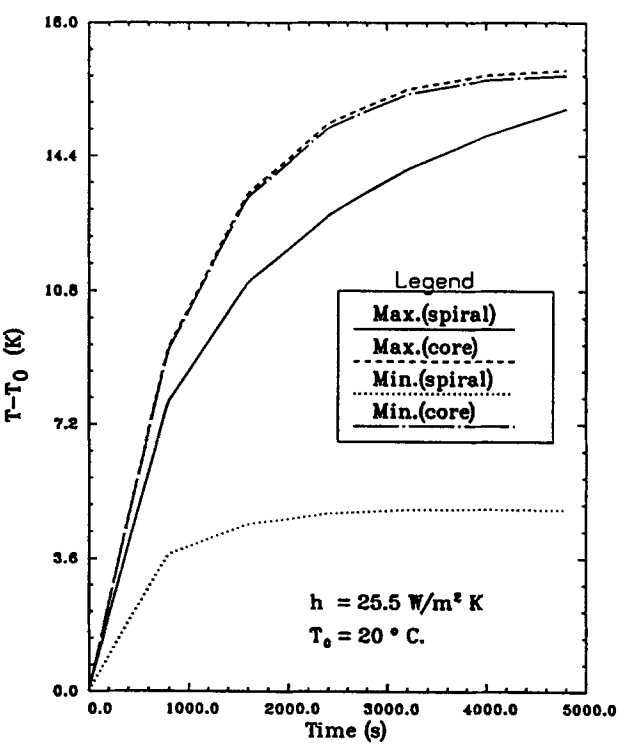

Fig. 12. A comparison of model predictions for a Li/BCX cell (5.37 mA/cm²) at 20°C ambient (T_0) using spiral and core models.

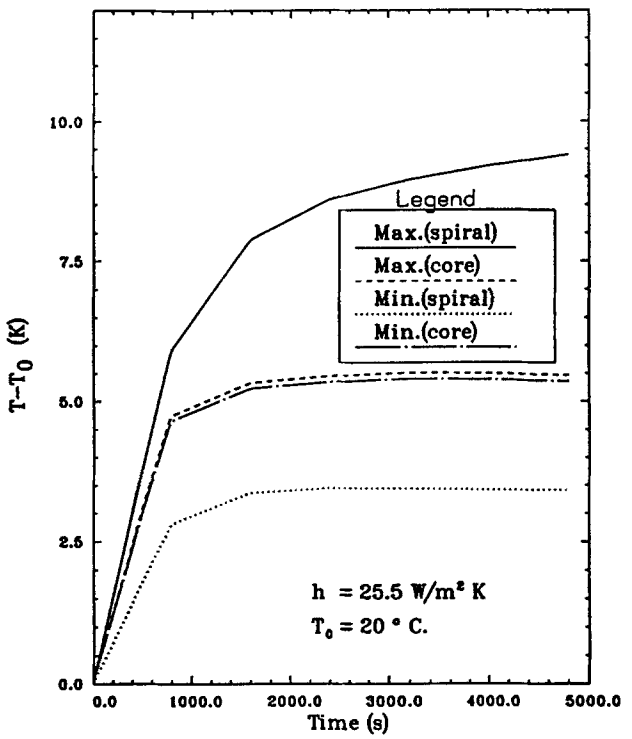

Fig. 13. A comparison of model predictions for a Li/$SOCl_2$ cell (1.89 mA/cm^2) at 20°C using spiral and core assumptions.

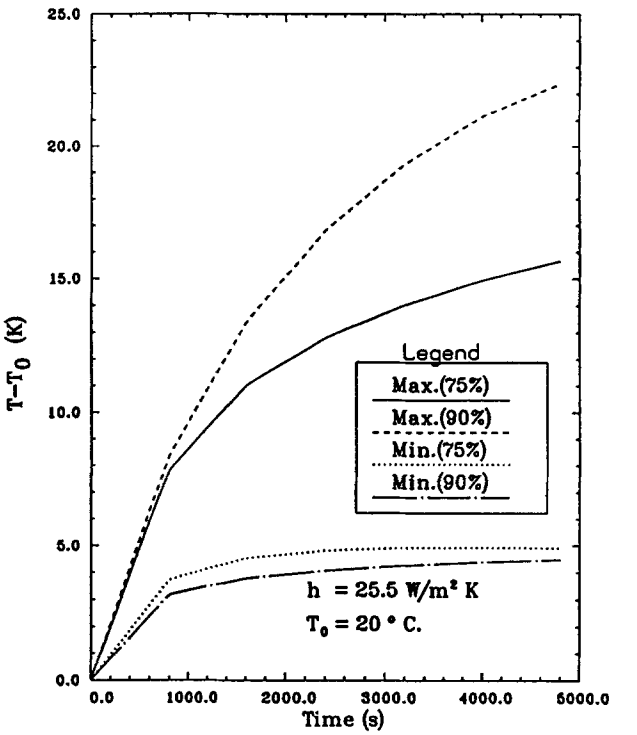

Fig. 14. Effects of assumed extent of reaction on the predicted maximum and minimum temperatures for Li/BCX cell (5.37 mA/cm^2) at 20°C ambient (T_o) using the spiral model.

The result shows that the closer the extent of the reaction is to unity (100%), the higher the maximum temperature predicted. However, a lower minimum temperature was predicted for the larger extent of conversion. The result further confirms the importance and the role of reaction products in the thermal behavior of the thionyl chloride based cells.

Conclusion and Recommendations

A thermal analysis of the Li/BCX and high rate Li/$SOCl_2$ cells was carried out. The thermal model developed was used to study the thermal behavior of BCX cells discharged at the same rate but at different ambient temperatures. The model predictions show that the ambient temperature of discharge plays a critical role in the thermal management of the cell. For convection cooling, the model prediction showed that an optimum ambient temperature for cell discharge should be close to the room temperature (25°C) for the lowest maximum temperature rise in the cell. The cell must be operated in a vacuum to eliminate convection heat transfer.

Inclusion of the effects of reaction products to the model shows that a constant composition assumption may be misleading. Heat transfer through the spiral constitutes a smaller fraction of the total heat dissipation from the cell. The thermal performance of a high rate Li/$SOCl_2$ cell was compared to that of a Li/BCX cell. The model was used to predict a higher temperature rise in the Li/$SOCl_2$ cell than in a Li/BCX cell discharged at the same rate. This was attributed to the differences in the reaction products of the two cells.

Several considerations that can be important in improving the model include the consideration of a complete mass and energy balance. The use of exact effective thermoneutral potentials at each ambient temperature can improve the model predictions. The vaporization of SO_2 and $SOCl_2$, chlorine and bromine produced on the dissociation of BrCl, must be accounted for to improve the model. The use of concentration and temperature dependent thermophysical properties can improve the model predictions. An appropriate thermal comparison of a Li/BCX cell with a Li/$SOCl_2$ cell requires using parameters of cells discharged at the same rate. The decrease in the thickness of lithium and the cathode swelling with reaction progress must be included for improved model predictions. The model also can be extended to three dimensions.

Manuscript submitted June 19, 1991; revised manuscript received Sept. 8, 1992.

Texas A&M University assisted in meeting the publication costs of this article.

LIST OF SYMBOLS

a	specific electroactive surface area of the porous electrode, m^{-1}
a°	initial value of a, m^{-1}
c_p	thermal capacity, J/kg/K
E_{etp}	effective thermoneutral potential, V
E_h	thermoneutral potential, V
E_l	cell load voltage, V
E_r	reversible cell potential, V
F	Faraday's constant, 96,487 C/mol
f_k	thermal conductivity of material k, W/m, K
I	current flow during cell discharge, A
L_m	thermal property of region m
q_{vj}	heat generation per unit volume from region, j, W/m^3
$s_{i,j}$	stoichiometric coefficient of species in reaction j
t	time, s
T	temperature, K
T_{sur}	temperature of the surrounding, k
T_w	temperature of outer wall of cell, T
v_{bi}	partial molar volume of species i, m^3/mol
X_i	mole or mass fraction of i
z_i	charge number of species i

Greek

ε_i	porosity of porous media i
ρ	density of electrolyte, g/cm^3
ρ_k	density of solid material k, kg/m^3
ψ	a dimensionless number

REFERENCES

1. N. A. Godshall and J. R. Driscoll, *This Journal*, **131**, 2221 (1984).
2. H. F. Gibbard, *ibid.*, **125**, 353 (1978).
3. L. A. Parnell and S. Szpak, *Electrochim. Acta*, **30**, 913 (1985).
4. T. I. Evans and R. E. White, *This Journal*, **136**, 2145 (1989).
5. Y. I. Cho, *ibid.*, **134**, 773 (1987).
6. J. J. Auborn, K. W. French, S. I. Lieberman, V. K. Shah, and A. Heller, *ibid.*, **120**, 1613 (1973).

7. R. M. Murphy, P. W. Krehl, and C. C. Liang, in *Proceedings of the 16th Intersociety Energy Conversion Engineering Conference,* Vol. 1 (1981).
8. B. J. Carter, R. M. Williams, F. D. Tsay, A. Rodriquez, S. Kim, M. M. Evans, and H. Frank, *This Journal,* **132,** 525 (1985).
9. K. M. Abraham, M. Alamgir, and S. Perrotti, *ibid.,* **135,** 2687 (1988).
10. S. Szpak, C. J. Gabriel, and J. R. Driscoll, *Electrochim. Acta,* **32,** 239 (1986).
11. Y. I. Cho and G. Halpert, *J. Power Sources,* **18,** 109 (1986).
12. E. E. Kalu, R. E. White, and E. C. Darcy, *This Journal,* **139,** 2755 (1992).
13. E. E. Kalu, R. E. White, and E. C. Darcy, *ibid.,* **139,** 2378 (1992).
14. K. A. Klinedinst, *ibid.,* **132,** 2044 (1985).
15. D. Bernardi, E. Pawlikowski, and J. Newman, *ibid.,* **132,** 5 (1985).
16. J. Lee, K. W. Choi, N. P. Yao, and C. C. Christianson, *ibid.,* **133,** 1286 (1986).
17. Y. Ogata, S. Kainuma, M. Yasuda, and F. Hine, *ibid.,* **132,** 2594 (1985).
18. T. Forland and S. K. Ratkje, *Electrochim. Acta,* **25,** 157 (1980).
19. Y. I. Cho and G. Halpert, in *Proceedings of the 32nd Power Sources Symposium,* Cherry Hill, NJ, June 9-12, 1986, The Electrochemical Society, Inc., p. 547 (1986).
20. S. Szpak and J. R. Driscoll, *J. Power Sources,* **10,** 343 (1983).
21. S. Gilman and W. Wade, *This Journal,* **127,** 1427 (1980).
22. C. C. Liang, P. W. Krehl, and D. A. Danner, *J. Appl. Electrochem.,* **11,** 563 (1980).
23. J. S. Dunning, Ph.D. Dissertation, University of California, Los Angeles, CA (1971).
24. J. S. Dunning, D. N. Bennion, and J. Newman, *This Journal,* **120,** 906 (1973).
25. IMSL, *PDE/PROTRAN: A System for the Solution of Partial Differential Equations,* 2nd ed., International Mathematical and Statistical Libraries, Inc., Houston (1989).
26. S. Szpak and H. V. Venkatasetty, in *Proceedings of the 13th International Power Sources Symposium held at Brighton (UK), Sept. 1982,* J. Thompson, Editor, Academic Press, London (1983).
27. A. J. Hills and N. A. Thompson, *J. Power Sources,* **24,** 253 (1988).
28. K. M. Abraham, L. Pitts, and W. P. Kilroy, *This Journal,* **132,** 2301 (1985).
29. W. D. K. Clark, Wilson-Greatbatch Ltd., Clarence, New York, Personal communications (1991).
30. E. Darcy, NASA JSC, Houston, Texas, Personal communications (1990).
31. *Chemical Engineers' Handbook,* 5th ed., R. H. Perry and C. H. Chilton, Editors, McGraw-Hill, New York (1987).
32. *CRC Handbook of Chemistry and Physics, Student Edition,* R. C. Weast, Editor, CRC Press, Inc., Boca Raton, FL (1987).
33. J. A. Dean, *Lange's Handbook of Chemistry,* 13th ed., McGraw-Hill Book Co., Inc., New York (1985).

Surface and Catalytic Properties of Iron-Platinum/Carbon Electrocatalysts for Cathodic Oxygen Reduction in PAFC

Kyong Tae Kim, Jung Tae Hwang, Young Gul Kim, and Jong Shik Chung

Department of Chemical Engineering, Pohang Institute of Science and Technology (POSTECH), Pohang 790-600, Korea

ABSTRACT

A Fe-Pt bimetallic catalyst was prepared by impregnating iron nitrate solution into a carbon-supported platinum catalyst. The catalyst was heat-treated in flowing Ar (nontreated) at 450°C (denoted as PF450), 750°C (PF750), and 900°C (PF900), or this process was followed by an acid-treatment in 1*M* H_2SO_4 solution to leach out surface-enriched iron (acid-treated). The surface and catalytic properties of these catalysts were studied using H_2-O_2 titration, XRD and TEM measurements, and oxygen reduction tests in PAFC. With increased heat-treatment temperature, the Pt surface area measured by hydrogen chemisorption (S_{CHEM}) decreases rapidly owing to particle sintering, alloying effect, and enrichment of iron on the surface. The mass activity (mA/g Pt) of the alloyed catalyst is about the same as that of pure Pt catalyst due to the particle sintering in the alloyed catalyst. However, the specific activity (mA/m^2 Pt, based on S_{CHEM}) of the alloyed catalyst is estimated at twice that of pure Pt catalyst. The acid-treatment leads to dissolution of surface-enriched iron and results in an increase of the Pt surface area due to surface roughening. Except for PF450, the specific activities of both nontreated and acid-treated catalysts are the same, indicating that S_{CHEM} is a good measure of active site for the reaction. After acid treatment of the partially alloyed PF750, a twofold increase in the Pt surface area (therefore, twice the increase in the MA) was observed when compared with the nontreated Pt-Fe alloy catalyst.

It has been claimed in recent patents[1-6] that alloying Pt with other metals, *e.g.,* transition metals such as Fe, Cr, Co, etc., enhances the activity of oxygen reduction in phosphoric acid fuel cells (PAFC). Wan[3] has claimed in a patent that Pt-Fe catalysts containing 25-40 atomic percent (a/o) Fe (with respect to Pt) show greater activity and better resistance to sintering. Luczak and Landsman have claimed that Pt-Cr[1] and Pt-Cr-Co [2,6] alloy catalysts exhibit twice the activity of a Pt catalyst. This activity was attributed to the formation of an ordered alloy of superlattice structure (Pt_3Cr). But Beard and Ross[7] have argued recently that this explanation of activity enhancement by alloying was flawed by ignoring the dependence of activity (either mass activity or specific activity) on the surface area of Pt, and that the magnitude of the enhancement is approximately 20%, not a factor of 2. They have suggested that the enhancement may be attributed to the surface roughness effect as suggested by Gottesfeld and coworkers[8-11] and/or to the creation of an active plane, *i.e.,* (100) vicinal plane of Pt,[12] not to the specific structure of alloy. Besides, Jalan and Taylor[13] have suggested that, by showing a linear relationship between specific activity and interatomic spacing on various Pt based alloy catalysts, geometric modification of Pt by alloying with foreign metals is a predominant factor on the alloying effect.

Meanwhile, it is well known that oxygen reduction on Pt in PAFC is a structure-sensitive reaction;[12,14-16] that is, activity is greatly dependent on particle size (surface area) of platinum. Therefore one other factor which should be considered is the catalysts surface composition because catalytic reaction depends on surface properties, not on bulk properties. The surface composition of alloy catalyst greatly differs from the nominal composition depending on the preparation conditions as well as the alloy system.[17-20]